International Journal of Heat and Mass Transfer 52 (2009) 2834–2848

Contents lists available at ScienceDirect

International Journal of Heat and Mass Transfer

journal homepage: www.elsevier.com/locate/ijhmt

Experimental investigations on heat transfer and frictional characteristics of a turbulator roughened solar air heater duct

Santosh B. Bopche [a,*], Madhukar S. Tandale [b,1]

[a] Department of Mechanical Engineering, Indian Institute of Technology Bombay, Powai, Mumbai, MS 400 076, India
[b] Department of Mechanical Engineering, Dr. Babasaheb Ambedkar Technological University, Lonere, MS 402 103, India

ARTICLE INFO

Article history:
Received 28 January 2008
Received in revised form 9 September 2008
Available online 13 February 2009

Keywords:
Turbulator
Solar air heater
Roughness
Heat transfer enhancement

ABSTRACT

An experimental investigation has been carried out to study the heat transfer coefficient and friction factor by using artificial roughness in the form of specially prepared inverted U-shaped turbulators on the absorber surface of an air heater duct. The roughened wall is uniformly heated while the remaining three walls are insulated. These boundary conditions correspond closely to those found in solar air heaters.

The experiments encompassed the Reynolds number range from 3800 to 18000; ratio of turbulator height to duct hydraulic mean diameter is varied from, $e/D_h = 0.0186$ to 0.03986 ($D_h = 37.63$ mm and $e = 0.7$ to 1.5 mm) and turbulator pitch to height ratio is varied from, $p/e = 6.67$ to 57.14 ($p = 10$ to 40 mm). The angle of attack of flow on turbulators, $\alpha = 90^\circ$ kept constant during the whole experimentation. The heat transfer and friction factor data obtained is compared with the data obtained from smooth duct under similar geometrical and flow conditions. As compared to the smooth duct, the turbulator roughened duct enhances the heat transfer and friction factor by 2.82 and 3.72 times, respectively. The correlations have been developed for area averaged Nusselt number and friction factor for turbulator roughened duct.

1. Introduction

When a flowing fluid comes in contact with a stationary surface, a thin viscous sublayer develops adjacent to the wall in turbulent boundary layers. "The viscous sublayer is defined as the thin layer in the vicinity of the wall in which the damping effect of the molecular viscosity on the turbulent velocity fluctuations is dominating. Such a layer is bounded from one side by a fixed wall, and bounded on the other side by a fluctuating and continuously changing flow, i.e., a flow of unknown structure and thickness". For the no slip condition, the velocity at the wall is zero. The universal logarithmic velocity profile in a turbulent boundary layer yields a zero velocity at a finite distance from the wall. The paradox can only be explained by the presence of a viscous sublayer. Such a sublayer has a linear velocity profile in the vicinity of the wall. Thus, in order to get the velocity profile across the whole boundary layer, two different equations are necessary, namely:

$$U^+ = Y^+ \;\&\; U^+ = B \cdot \log Y^+ + C \quad \text{where,} \quad U^+ = \sqrt{U/U_\tau} \quad \text{and} \quad Y^+ = Y\frac{U\tau}{v}$$

The point of intersection of these two velocity profiles is defined in the literature as the 'nominal thickness of the viscous sublayer', which depends upon the shape and size of the surface roughness as well as the pressure gradient in the flow direction [1]. In a very thin layer in the vicinity of wall, conduction process is predominant. Beyond this, heat transfer process is dominated by convention. Heat transfer rate in this viscous sublayer is adversely affected due to lower thermal conductivity and relatively low velocity of air.

One of the methods to overcome this problem is provision of artificial roughness in the form of interruptions in flow path to restrict the development of viscous and thermal boundary layer and promote turbulences, rather than increase the heat transfer area. This technique is mainly used in internal cooling passages for turbulent gas flows, apart from that it is giving better performance in solar air heaters (Reynolds number, $Re \leqslant 12{,}000$). Inclusion of artificial roughness, however, results in higher friction factor and consequently the higher pumping power. The surface roughness can be produced by several methods, like sand blasting, machining, casting, forming, pasting ribs, dimples, scales, fixing thin circular wires and by using expanded metal mesh over the surface; orienting ribs transverse, oblique, V-shaped either upstream or downstream to the flow or arranging parallel or discrete manner on the heat transfer surface. Ribs of different cross-sections like semicircular, triangular, square, rectangular, trapezoidal, wedge shaped or chamfered ribs and circular wires have been examined so far.

* Corresponding author. Tel.: +91 9892 518668.
E-mail addresses: santoshb.bopche@yahoo.co (S.B. Bopche), tandale1@yahoo.com (M.S. Tandale).
[1] Tel.: +91 2140 275 117; fax: +91 2140 275 142, +91 2140 275 040.

0017-9310/$ - see front matter © 2009 Elsevier Ltd. All rights reserved.
doi:10.1016/j.ijheatmasstransfer.2008.09.039

Nomenclature

A	hot surface area [m^2]
A_o, B_o, B, C	constants
Cp	specific heat of air [J/kg K]
d	gap distance from side edge of absorber/heater [m]
D, D_h	hydraulic mean diameter of test duct [m]
e	turbulator tip height or height of turbulator tip above roughened wall surface or rib height
f	average friction factor
g	gap width [m]
h	convective heat transfer coefficient [W/m^2 K]
h_m	manometric difference [mm]
H	depth of duct [m]
K_{air}	'thermal conductivity of air [W/m K]
l	projected length of metal grit perpendicular to direction of flow [m]
L	test duct length [m]
m'	mass flow rate of air through the test duct (kg/sec)
p	pitch of Turbulator as roughness element [mm]
P	perimeter of test duct [m]
ΔP	pressure drop in the test duct [N/m^2]
q''	heat flux [W/m^2]
Q_u	useful heat gain [Watt]
s	projected length of metal grit parallel to direction of flow, m
T_{fo}	fluid temperature at exit of test duct [°C]
T_{fi}	fluid temperature at inlet of test duct [°C]
T_b	bulk mean temperature of air [°C]
T_{pavg}	average Temperature of heater foil [°C]
U	velocity [m/s]
$U\tau$	shear velocity, $\sqrt{\tau_w/\rho}$
V_{air}	average velocity of air [m/s]
W	width of duct, [m]
X/Y	coordinates in flow direction/normal

Dimensionless parameters

d/W	relative gap position
e/D_h	ratio of turbulator tip height to hydraulic mean diameter
e^+	roughness Reynolds number
g/e	relative gap width
g/p	relative groove position
Nu	average Nusselt number
p/e	ratio of turbulator pitch to its tip height or relative roughness pitch in case of rib-roughness
Pr	Prandtl number
Re	Reynolds number
St	Stanton number
W/H	duct aspect ratio

Greek symbols

α	angle of attack of air on roughness elements
δ'	transition sublayer thickness [m]
Φ	rib chamfer angle
φ	rib wedge angle
η	performance parameter
μ	dynamic viscosity of air [Ns/m^2]
ν	kinematic viscosity of air [m^2/s]
θ	manometric limb inclination, 8°
ρ	density of air [kg/m^3]
ω	width of rib
τ	shear stress at the surface

Subscripts

r	rough duct
s	smooth duct
w	wall surface

Applications include fuel rods of gas cooled nuclear reactors, inside cavities of gas turbine blades, internal surfaces of pipes and plates in heat exchangers, electronic equipments, shipping machineries (in large scale marine boiler), combustion chamber liners, missiles, re-entry vehicles, ship hulls and piping networks, and solar air heaters. Nikuradse, who conducted a series of experiments with pipes roughened by sand grains, performed an early study of the effect of roughness on friction and velocity distribution, in 1933. Han et al. [2] studied the effects of ribs shape, angle of attack and pitch to height ratio on friction factor and heat transfer.

For solar air heater applications, Prasad and Saini [3] have investigated the effect of small diameter protrusion wire roughness on its performance for fully developed turbulent flow. Experimental investigation has been carried out [4] to determine the effect of transverse wire roughness on heat and fluid flow characteristics in transitionally rough flow region (e^+ = Roughness Reynolds number, $5 < e^+ < 70$) for rectangular solar air heater ducts with an absorber plate. It is concluded that the behavior of Stanton number in a transitionally rough flow region is different from its behavior in a fully rough region. Varma and Prasad [5] have used thin copper wires on the bottom side (flow side) of the absorber plate of a solar air heater and reported optimal thermo hydraulic performance, $\eta_{thermo} = 71\%$ corresponding to the roughness Reynolds number, $e^+ = 24$. Later, Gupta et al. [6] have observed that non-transverse ribs are advantageous and attains a maximum value of heat transfer for an angle of attack of 60° when compared with transverse ribs.

Sahu and Bhagoria [7] have investigated the effect of 90° broken wire ribs on heat transfer coefficient of a solar air heater duct. A pitch of 20 mm gives the highest thermal efficiency of 83.5% for e = 1.5 mm and reported heat transfer coefficient of roughened duct 1.25–1.4 times compared to smooth duct under similar operating conditions at higher Reynolds number. Abdul-Malik et al. [8] have conducted tests using V-shaped rib-roughness in the form of fine wires on the heat-transferring surface and reported a better performance for an angle of attack of 60° V-shaped ribs. A computational analysis (using CFD software, FLUENT 6.1) of heat transfer augmentation and flow characteristics due to artificial roughness in the form of ribs (Rectangular, Square, Chamfered, Semicircular and Circular) on a broad wall of rectangular duct for turbulent flow is also available in the literature [9]. The main findings are: (1) the angle ribs give highest heat transfer enhancement but at the cost of very high friction factor specifically at low Reynolds numbers, (2) the rectangular and square ribs give high heat transfer with moderate pressure penalty, (3) the circular and semicircular ribs show good performance from friction point of view but give low heat transfer enhancement in comparison to other rib-shapes, (4) higher Nusselt number is found in chamfered ribs than rectangular ribs. Experimental investigations [10,12] show that Nusselt number can be further enhanced beyond that of ribbed duct keeping friction penalty low by using rib-grooved artificial roughness. The maximum heat transfer occurs for a relative roughness pitch, 'p/e' of about 6.0 and the optimum condition for heat transfer occurs at a groove position to pitch ratio, 'g/p' of 0.4, while on the either side of this ratio, both Nusselt number and friction factor decreases.

Bhagoria et al. [11] have studied the effect of transverse wedge shaped rib-roughness on the solar air heater performance for rib wedge angle (Φ) of 8°,10°,12° and 15° and reported maximum heat transfer enhancement for wedge angle of about 10°. The friction factor shows an increasing trend with wedge angle. Application of expanded metal mesh on the absorber surface also yields appreciable results [13].

Karwa et al. [14] have investigated experimentally the effect of roughness height ratio, relative roughness pitch, rib head chamfer angle of repeated chamfered rib-roughness and effect of duct aspect ratio on heat transfer and friction factor in solar air heater. A 15° chamfered ribs yield the maximum heat transfer and also the friction factor. Karmare and Tikekar [15] have reported two fold enhancements in the Nusselt number and three fold rises in friction factor over smooth duct with metal grit ribs of circular cross section in staggered manner for solar air heaters. They observed that the plate of roughness parameters, $l/s = 1.72$, $e/D_h = 0.044$, $p/e = 17.5$ shows optimum performance. The effects of gap (gap width, 'g/e' and gap position, 'd/W' ratios) in an inclined (60°) continuous square rib arrangement on the performance of solar air heater have been studied by Aharwal et al. [16]. The duct has width to height ratio (W/H) of 5.84, $p/e = 10$, roughness height ratio, $e/D_h = 0.0377$, and angle of attack (α) of 60°. The gap width, 'g/e' and gap position, 'd/W' is varied from 0.5 to 2.0 and 0.167 to 0.67, respectively for Re, 3000 to 18,000. The maximum enhancement in Nusselt number and friction factor is observed to be 2.59 and 2.87 times the smooth duct, respectively yielding maximum performance parameter for the relative gap width of 1.0 and the relative gap position of 0.25.

For electronics cooling application, Pfahnl et al. [17] have described a new design feature for integrated circuit test handler tray by incorporating lateral ribs that significantly increases the rate of convective heat transfer to the tray and the devices of the tray. In addition to the above discussed roughness geometries, the use of dimples on the absorber surface also reported a significant improvement in performance [18]. Detailed analysis of optimization of roughness and flow parameters (p/e, e/D, Re) to maximize heat transfer while keeping friction losses minimum is available [19]. It shows that a parameter known as Roughness Reynolds number, ($e^+ = e/D\sqrt{f_r/2}\cdot Re$) combining the roughness and flow parameters both attain a particular value at which optimal thermo hydraulic performance could be achieved. For aspect ratio, $W/H >> 1$ (W = width of duct and H = depth of duct), $p/e \geqslant 10$ and 'e/D' is chosen such that the roughness height is of the order of or slightly greater than laminar sub-layer thickness; it is found that the optimized conditions always correspond to a fixed value of roughness Reynolds number, $e^+_{opt} \cong 24$. Chandra et al. [20] have studied the heat transfer and friction characteristics for the applications of turbulent internal channel flows involving different number of rib roughened walls.

The effect of rib angle of attack and the channel aspect ratio on the distribution of the local heat transfer coefficient for developing flow in short rectangular channels has been studied by Han [21–24] for Reynolds number from 10,000 to 60,000. The concept of combined turbulence promoters in the form of rib-groove, with groove at the center of ribs was introduced by Zhang et al. in 1994 [25]. The effects of ridge shapes (semicircular, triangular and square), arrangement of continuous ribs and that of discrete rib turbulators on heat transfer and friction factor is also available in the literature [26–28]. It is reported that the semicircular and triangular ridge geometries are less likely to yield the hot spots behind the ridges than the square one. The highest heat transfer is reported for the 60° rib pattern due to the strong rotational momentum of the secondary flow. Ten to fifteen percentage of heat transfer enhancement is reported in case of discrete rib arrangement over 90° transverse continuous ribs. The most important work is done by Liou and Hwang [29] to locate the peaks of heat transfer enhancement and the region susceptible to hot spots, to determine the relative contribution of the rib surface and the channel wall to the heat transfer augmentation and to develop compact correlations, using a laser holographic interferometer and thermocouples. Roughened duct rotational effects are seemed to be more pronounced in turbulated passages of high aspect and low blockage ratios (e/D_h) for which a steady increase in heat transfer coefficient is observed, for 45° criss–cross ribs on two opposite walls by Taslim et al. [30]. The study of the effect of transverse, angled ribs, discrete, angled discrete ribs, V-shaped, V-shaped broken and parallel broken ribs on heat transfer and friction appears in [31–34]. It is seen that 90° transverse ribs represent the lowest thermal performance, based on the same pumping power. The 60° parallel broken ribs or 60° V-shaped broken ribs provide a higher heat transfer augmentation than the 45° parallel broken ribs or 45° V-shaped broken ribs. Parallel angled discrete ribs are superior to parallel angled full ribs. Parallel 60° discrete ribs have the highest ribbed wall heat transfer. The heat transfer augmentation is also observed in a channel with deep dimples, protrusions and scale-roughened walls [35–37]. Theoretical and numerical work in this direction has also been reported in the literature [38–40].

The researchers reported that in case of ribs at low Reynolds number (less than 5000), the value of Nusselt number for the smooth duct is nearly equal to that of rough duct. It is also concluded that smooth duct gives better heat transfer than the artificially roughened duct with ribs at low Reynolds number [7]. It is also reported that for low Reynolds number flow, change in heat transfer coefficient is negligible with respect to roughness pitch, because when Re is low the thermal boundary layer remains unbreakable, which offers resistance to heat flow and hence it may result low heat transfer coefficient [11]. Common drawback revealed from the literature on ribs, is the formation of eddies upstream and downstream of it, which create more losses in the flow and also affects the heat transfer enhancement. It may be the reason of poor heat transfer enhancement at low Reynolds number. Carving ribs of required shape on the absorber plate demands skill work and expensive machining. Keeping in mind above constraints a new kind of turbulator is prepared in order to eliminate the formation of eddies thereby to increase the heat transfer rate, even at low Reynolds number.

Using inverted U-shaped turbulator, optimally 59% more heat transfer enhancement at the cost of 122.7% more friction penalty was observed, encompassing experiments for the Reynolds number range of 1000–5000, turbulator tip height to duct hydraulic mean diameter ratio, $e/D_h = 0.03986–0.2$ ($D_h = 37.63$ mm and $e = 1.5–7.5$ mm) and turbulator pitch to its tip height ratio, $p/e = 10.42–33.33$ [41]. Since, the present geometry has given significant heat transfer enhancement in low Reynolds number flow compared to that of ribs; it was decided to investigate the performance of same inverted U-shaped turbulator geometry in higher Reynolds number flow (Re = 3800–18,000).

2. Experimental details

2.1. Experimental apparatus

An experimental set-up has been designed and fabricated to study the effect of inverted U-shaped turbulators on heat transfer and fluid flow characteristics in rectangular duct. In Solar air heaters, the roughness elements have to be considered only underside of one broad wall, which receives the solar radiation. Therefore, the solar air heaters are modeled as a rectangular channel having one rough wall and three smooth walls. A schematic diagram of the experimental set-up including the test duct cross section is shown in Fig. 1. The test apparatus is an open air flow loop that consists of

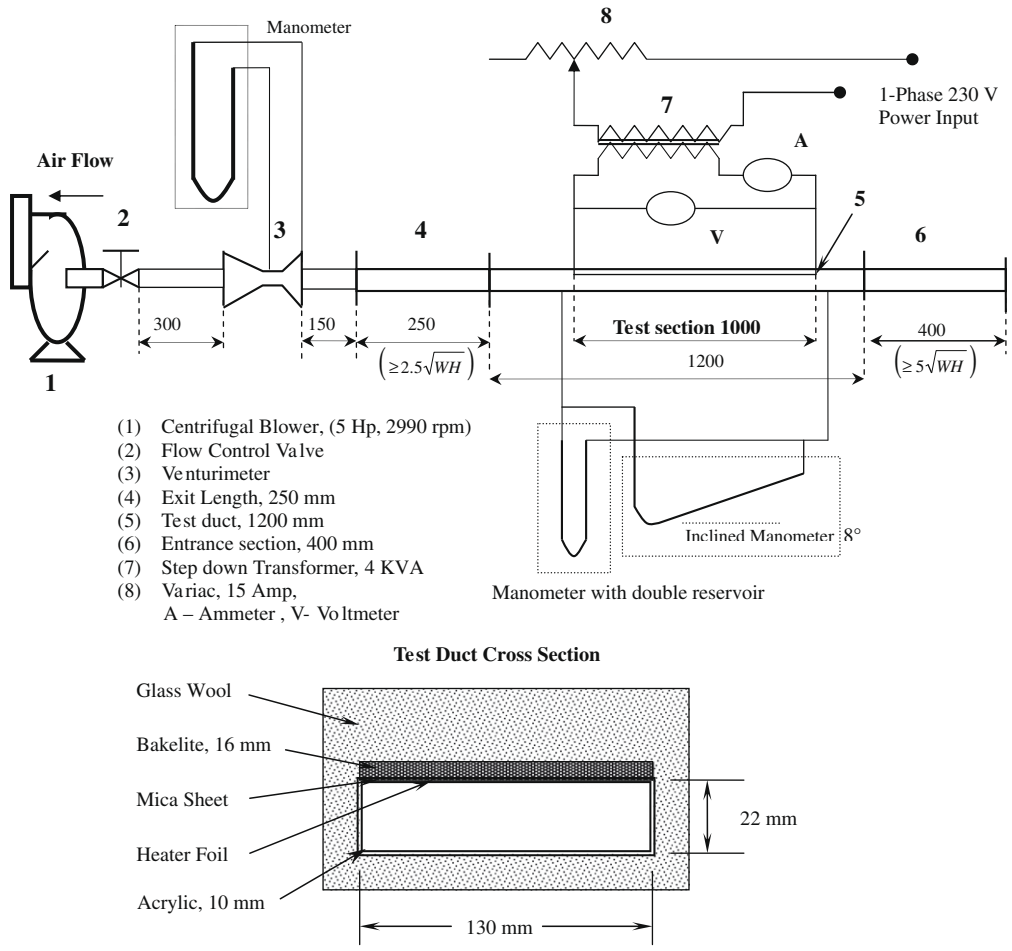

Fig. 1. Schematic diagram of experimental set-up with test duct cross-section.

a centrifugal blower (1), flow control valve (2), Venturimeter (3) (for flow measurement), an entrance section (6), the test section (5), and an exit section (4).

The duct is of size $1850 \times 130 \times 22$ mm (dimensions of inner cross section) and is constructed from Acrylic sheet of 10 mm thickness. The Test section is of length 1000 mm ($29.16D_h$). The exit and entry lengths are 250 mm ($6.64D_h$) and 400 mm ($10.63D_h$), respectively. A short entrance length is chosen because for a roughened duct, the thermally fully developed flow is established in a short length 2–3 times of hydraulic diameter. For the turbulent flow regime, ASHRAE standard 93–77 recommends entry and exit length of $5\sqrt{WH}$ and $2.5\sqrt{WH}$, respectively. The exit section of 250 mm is used after the test section in order to reduce the end effects. To provide uniform heat flux, electric heater of size 1000×136 mm is fabricated by a Stainless Steel foil (Grade 304), 0.05 mm thickness, itself is acting as a roughened surface. The heater is located at the top wall while the remaining three walls are insulated so as to simulate the solar air heater duct. A mica sheet of 0.5 mm is sandwiched between the electric heater and the Bakelite plate. The top wall is made of Bakelite plate of 16 mm thickness so as to minimize the top loss. The temperature of the heater foil is sensed by the thermocouples situated between the mica and bakelite. Fig. 4 shows the position of the thermocouples in the test duct. In order to improve the accuracy of temperature measurement and to prevent sagging of heater, SS foil is pasted firmly to the mica sheet and mica to bakelite. Thermal resistance offered by very thin mica sheet (0.5 mm) is found to be negligible. The whole periphery of the test duct and the exit section is covered by a Glass wool layer of 10 and 5 cm thickness at the top and sides of the duct, respectively, in order to minimize the heat loss to the surrounding. The mass flow rate of air is measured by a Venturimeter and the Gate Valve provided in the line controls the flow. For measurement of pressure drop across the Venturimeter a U-tube manometer, with Carbon Tetrachloride (CCL_4) as a manometric fluid, is used. The calibrated K-type thermocouples (0.3 mm i.e. 24 SWG) are used for the measurement of the average air temperature at inlet and outlet and the heated foil temperatures at different locations. Two thermocouples for inlet air temperature, three for exit air temperature, and ten thermocouples for the temperature of the heater, are used. Four additional thermocouples are inserted in the Bakelite plate to measure the heat loss from top of the duct. The cold junctions of the thermocouple are held at zero degree Celsius by using a thermo-flask containing an ice–water mixture. A digital milli-voltmeter is used for the output of thermocouples. A voltage drop across the heater is measured by means of a digital voltmeter. The pressure drop across the rough test section is measured by a 'U-tube manometer with double reservoir' (range = 0.002–5 mbar) and for smooth duct 8° inclined U-tube manometer with double reservoir', filled with Benzyl Alcohol and water, is used. An inverted U-shaped turbulator is prepared in such a way that more number of sharp edges can be provided to shear the viscous boundary layer as shown in Fig. 2. The turbulators are cut from thin aluminium sheet of 0.3 mm thickness and pasted underside the heater surface as shown in Fig. 3. The range of roughness and flow parameters covered in the present study is as given in Tables 1 and 2.

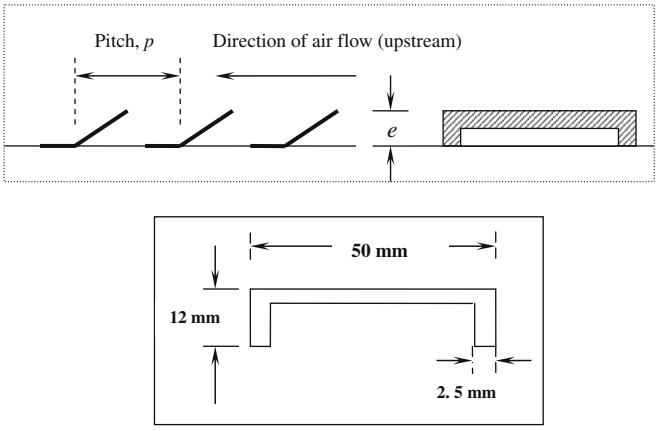

Fig. 2. Turbulator geometry.

2.2. Experimental procedure

After fixing the turbulators, test section is assembled and checked for air leakage. The blower was switched on to let a predetermined rate of airflow through the duct. The test section was then heated to maintain the heater temperature near the exit at least 15 °C above the exit air temperature, to get accurate heat transfer coefficient value and also keeping in mind the safe working temperature limit of Acrylic (~100 °C). The heat flux is the rate of net heat input divided by the heat transfer area (without considering turbulator surface area). The net heat flux and the average heater to bulk mean air temperature difference was determined over a test section. Six values of flow rates were used for each set at same or fixed uniform heat flux. At each value of flow rate and the corresponding heat flux, system was allowed to attain a steady state before the temperature data were recorded. Having adjusted the heater power or the air flow rate, the corresponding steady state was assumed when no considerable variations of heater surface temperatures between several successive scans being observed, for 10–15 minutes. The pressure drops were measured at no heat input condition.

During experimentation the following parameters were measured:

1. Pressure difference across the venturimeter.
2. Temperature of the heated surface and temperatures of air at inlet and outlet of the test section and
3. Pressure drop across the test section.

2.3. Data reduction

Mass flow rate of air is determined from the pressure drop across the venturimeter, using a following relation:

Table 1
Range of flow and roughness parameters.

Reynolds number, '*Re*'	3800–18,000
Turbulator height to hydraulic mean diameter ratio, 'e/D_h'	0.0186–0.03986
Turbulator pitch to height ratio, 'p/e'	6.667–57.14
Angle of attack of flow, 'α'	90°
Duct aspect ratio, 'W/H'	6

$$m' = \left(C_d \rho_{air}(a_1 a_2) \Big/ \sqrt{(a_1^2 - a_2^2)}\right) \sqrt{2g \cdot h_{m,CCL_4}} \quad (1)$$

where,

a_1 Inside area of cross section of pipeline,
a_2 Area of cross section of venturi-throat,
C_d Coefficient of discharge of Venturimeter (0.946 for $Re \sim 10{,}000$).

The useful heat gain of the air is calculated as:

$$Q_u = m' C_p (Tf_o - Tf_i) \quad (2)$$

The heat transfer coefficient for the test section is:

$$h = Q_u / A \cdot (T_{pm} - T_{fm}) \quad (3)$$

where, T_{pm} is the average value of the heater surface temperatures, T_{fm} is the average air temperature in the duct = $(Tf_i + Tf_o)/2$

The Nusselt number as,

$$Nu = h \cdot D_h / K_{air} \quad (4)$$

The friction factor was determined from the measured values of pressure drop across the test length, $L = 1$ m using:

$$f = (\Delta P) D_h / (2 \rho_{air} L V_{air}^2) \quad (5)$$

The thermo-physical properties of air used in the calculation of heat transfer and friction parameter were taken from a text by Duffie and Beckman [42] corresponding to mean bulk air temperature. Further the effect of humidity on thermo-physical properties has been neglected since the change in relative humidity values during the experimentation was insignificant. The maximum possible measurement errors in the values of major parameters of present investigation are, Reynolds number, $Re \pm 1.25\%$, Nusselt number, $Nu \pm 2.63\%$ and friction factor, $f \pm 4.75\%$.

3. Validity tests

The basic purpose of validity test is to serve as a basis of comparison of results with the values for heat transfer and friction factor from correlations available for smooth duct in the literature. The Nusselt number and friction factor determined from these experimental data are compared with the values obtained from the correlations i.e. Dittus–Boelter correlation (Kays and Perkin, 1990), the Blasius equation and the Karman–Nikuradse equation

Fig. 3. Photograph of turbulator roughened absorber plate.

Table 2
Parameters of turbulator geometry (D_h = 37.63 mm).

p (mm)	10	10	10	20	20	20	30	30	30	40	40	40
e (mm)	0.7	1.0	1.5	0.7	1.0	1.5	0.7	1.0	1.5	0.7	1.0	1.5
e/D_h	0.018	0.026	0.039	0.018	0.026	0.039	0.018	0.026	0.039	0.018	0.026	0.039
p/e	14.28	10	6.67	28.57	20	13.33	42.85	30	20	57.14	40	26.67

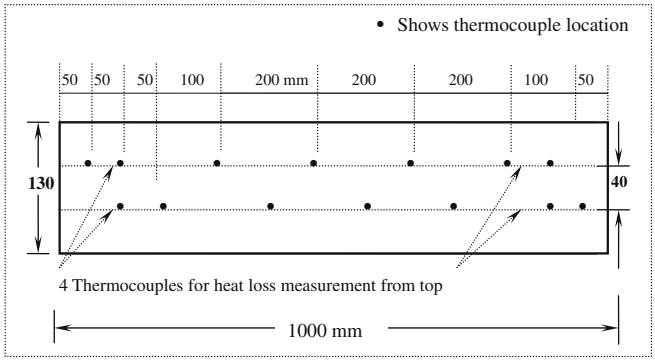

Fig. 4. Location of thermocouples on the heater.

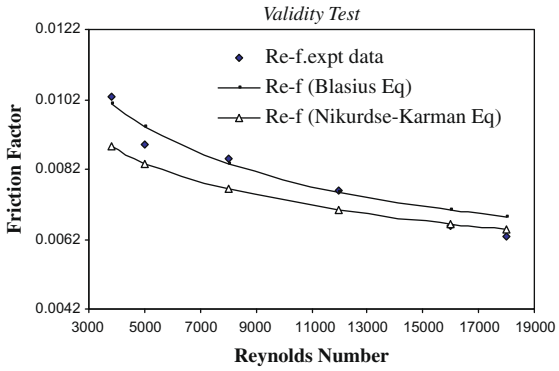

Fig. 6. Friction factor vs. Reynolds number for smooth duct.

for friction factor, are given below. The comparison is shown in Figs. 5 and 6.

$$\text{Dittus–Boelter equation}: Nu_s = 0.023Re^{0.8}\,Pr^{0.4} \quad (10^4 \le Re \le 1.24\times10^5) \tag{6}$$

$$\text{Blasius equation}: f_s = 0.0791Re^{-0.25} \quad (4\times10^3 < Re \le 10^5) \tag{7}$$

$$\text{\& Karman–Nikuradse equation}: f_s = 0.046Re^{-0.2} \quad (3\times10^4 < Re \le 10^6) \tag{8}$$

The average absolute percentage deviation of the present experimental Nusselt number data is ±8.27% (Maximum Deviation is ±12.14%) from the values predicted by Eq. (6), and the average absolute percentage deviation for friction factor data is ±3.82% (maximum deviation = ±6.82%) from the values predicted by Eq. (7). The validity test friction factor data for smooth duct is also compared with Karman–Nikuradse Eq. (8). The average absolute percentage deviation for friction factor data is ±10.43% (maximum deviation = ±17.98%).

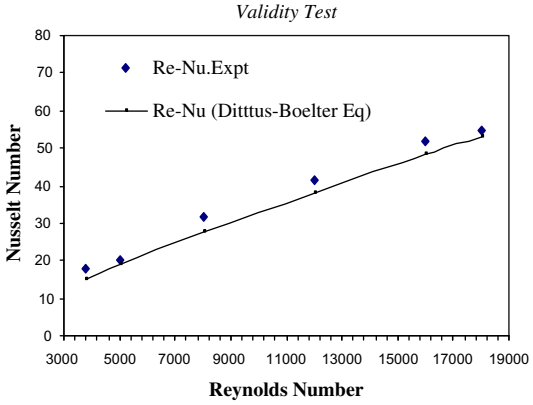

Fig. 5. Nusselt number vs. Reynolds number for smooth duct.

4. Results and discussion

Using the data obtained from experiments, the heat transfer, friction factor and the thermal performance characteristics of duct are discussed in the following subsections.

4.1. Heat transfer and friction factor

Fig. 7 shows the variation of Nusselt number for turbulator roughened and smooth duct with a wide range of relative roughness pitch and Reynolds number for p = 10, 20, 30 and 40 mm. The values of Nusselt number were found to increase with increasing Reynolds number in all cases as expected. The turbulator roughened duct yield maximum Nusselt number at pitch-height ratio, 'p/e' of 6.67 (p = 10 and e = 1.5 mm) as compared to higher roughness pitch values for the selected range of variables of experimentation.

It was also seen that Nusselt number decreases with increasing relative roughness pitch values. The data points are plotted for different pitches at three turbulator tip heights, e = 0.7, 1.0 and 1.5 mm. At low pitches with small variation of turbulator tip height, Nusselt number shows an appreciable variation. The effect of relative roughness pitch and Reynolds number on friction factor of turbulator roughened duct for a wide range of roughness pitches, as indicated in Table 2 is shown in Fig. 8. It was seen that the value of friction factor decreases with increasing Reynolds number in all cases as expected due to the suppression of viscous sub-layer. Also friction factor decreases with increase in relative roughness pitch value. It was observed that, a pitch to height ratio of 6.67 (p = 10 and e = 1.5 mm) has maximum friction factor and that of 57.143 has a minimum value for the selected range of pitch-height ratio values. The height of turbulator was restricted by the friction penalty, $[f_r/f_s]$ so as to keep performance parameter, 'η' within acceptable range.

The data of Fig. 7 has been re-plotted in Fig. 9 to bring out the effect of Reynolds number wherein it can be again seen that the Nusselt number increases with increase in Reynolds number and decreases with increase in relative roughness pitches. With this kind of turbulator, the roughened duct is showing significant heat transfer enhancement as compared to that of smooth duct at low Reynolds number too (Re < 5000). Fig. 10 shows the effect of Rey-

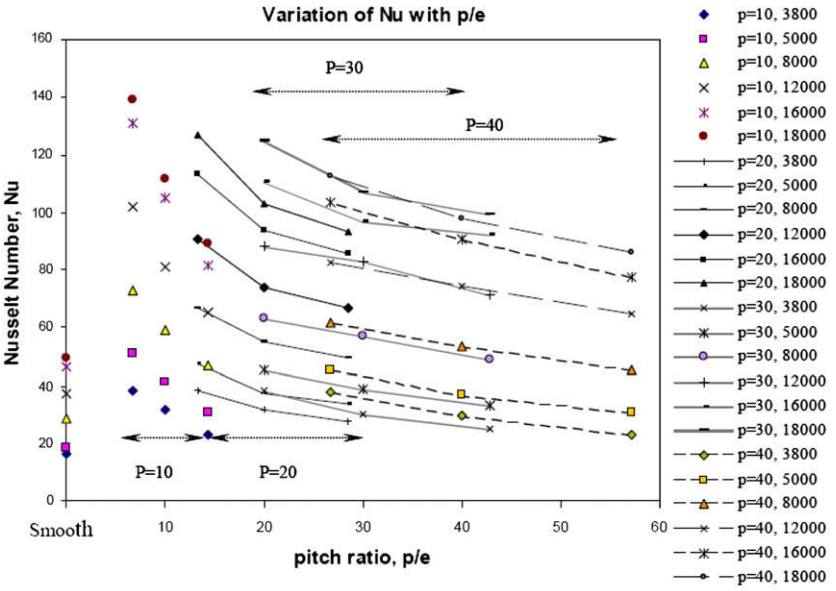

p	10	10	10	20	20	20	30	30	30	40	40	40
e	1.5	1	0.7	1.5	1	0.7	1.5	1	0.7	1.5	1	0.7
e/Dh	0.0398	0.026	0.0186	0.0398	0.026	0.0186	0.0398	0.026	0.0186	0.0398	0.026	0.0186
p/e	6.667	10	14.286	13.33	20	28.57	20	30	42.86	26.667	40	57.143

Fig. 7. Trend of Nusselt number as a function of pitch ratio (p/e = 6.67 to 57.143).

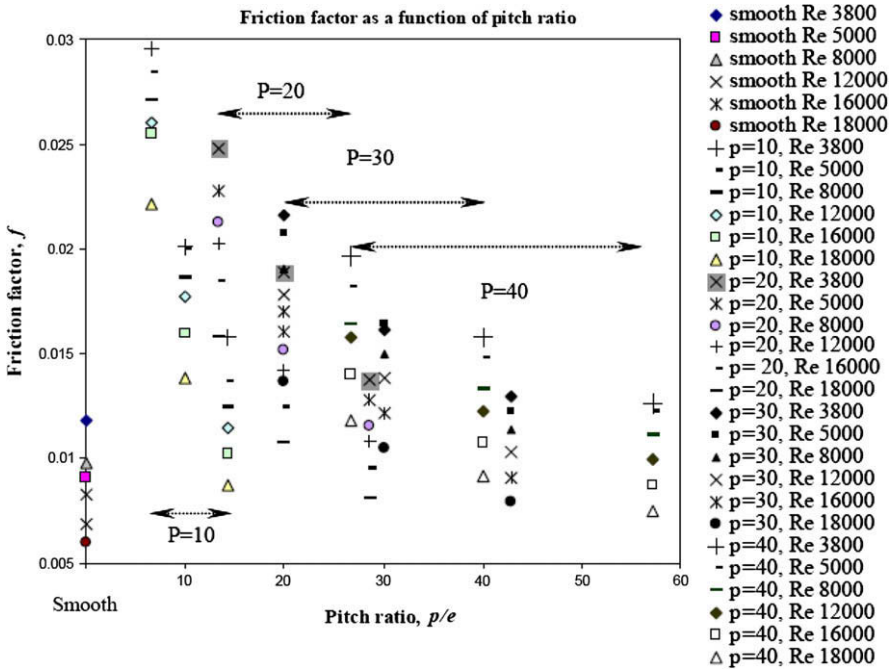

Fig. 8. Trend of friction factor as a function of pitch ratio (p/e = 6.67–57.143).

nolds number and relative roughness pitch on friction factor in the range of Reynolds number investigated for fixed value of other parameters. It was seen that the value of friction factor decreases with increasing Reynolds number in all the cases. The friction factor is showing maximum value at pitch-height ratio of 6.67 for the selected range of turbulator pitch-height ratios.

Only the difference between the ribs and the present turbulators is that optimum point of the roughness pitch could not be observed with turbulators. It shows continuous rise in Nusselt number and friction factor with reducing pitches, even less than the pitch-height ratio, 'p/e' of 10 i.e. at p/e = 6.67 also it shows rise in these parameters. It is an advantage with this geometry; maximum possible heat transfer enhancement can be acquired at affordable friction loss.

From the curves of same pitch ratio p/e = 20, but different pitches and turbulator tip heights, it was seen that the geometry

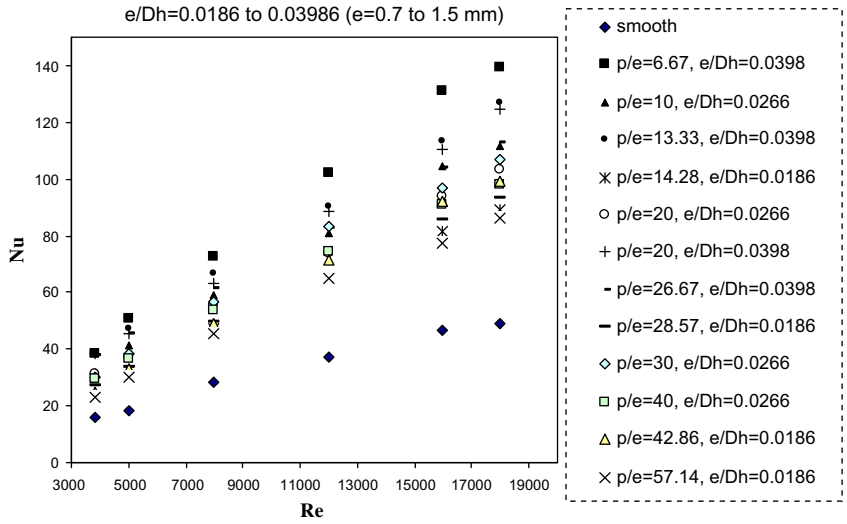

Fig. 9. Variation of Nusselt number as a function of Reynolds number.

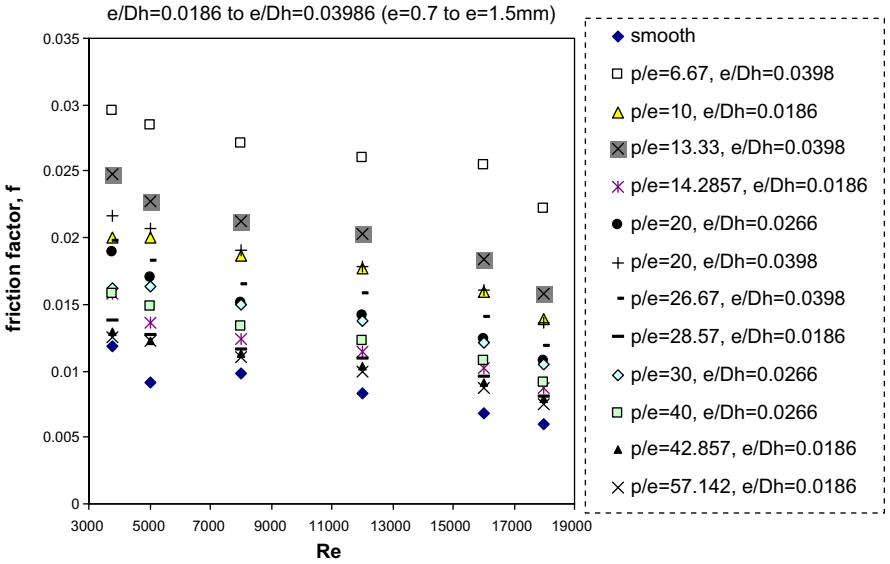

Fig. 10. Variation of friction factor as a function of Reynolds number for various pitch ratios.

having more roughness height is severely affecting the performance of the duct rather than having less pitch, shown in Fig. 11. Figs. 12 and 13 show the variation of Nusselt number and friction factor as a function of Reynolds number for inverted U-shaped turbulators having fixed values of turbulator tip height-hydraulic diameter ratio, 'e/D_h' and different pitch-height ratios, 'p/e'. It can be seen from these figures, that the Nusselt number values increase with increase in Reynolds number, whereas the friction factor decreases with increase in Reynolds number that is similar to the previous discussion. It is also seen that there is no much effect of roughness pitch on Nusselt number at lower values of Reynolds number but it is otherwise for friction factor.

Literature reveals an optimum 'p/e' values in the range of 8–10 specifically for ribs. But with this kind of turbulators Nusselt number increases continuously with reducing pitch ratio values which may be attributed to the passage provided underside the turbulator which allows higher velocity air to accelerate and approach the hot surface and allow it to flow underway rather than to circulate upstream and down stream of turbulator which invite eddies to form, and ultimately reduce the heat transfer in case of ribs. Partial obstruction of flow and more number of cutting edges are the specialties of the present turbulator, which creates low friction penalty compared to the rib geometries.

Several researchers have studied the performance of ribs in cooling applications including solar air heaters. Since, solar air heaters operate under low Reynolds number range (up to 12,000), a rigid roughness geometry like ribs can easily be replaced by turbulators. In particular, an inverted U-shaped turbulator is advantageous to ribs in some aspects like:

1. Provision of ribs completely obstructs the viscous sub-layer adjacent to the hot wall, which generates eddies/recirculation zones upstream and downstream of it as shown in Fig. 14 (a–c). Eddies not only reduce the heat transfer but also increase the pressure drop. With opening the passage downstream the

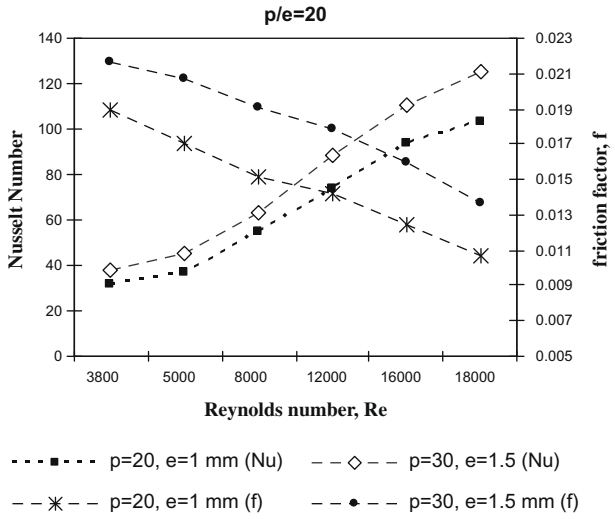

Fig. 11. Variation of friction factor as a function of reynolds number for ($p/e = 20$).

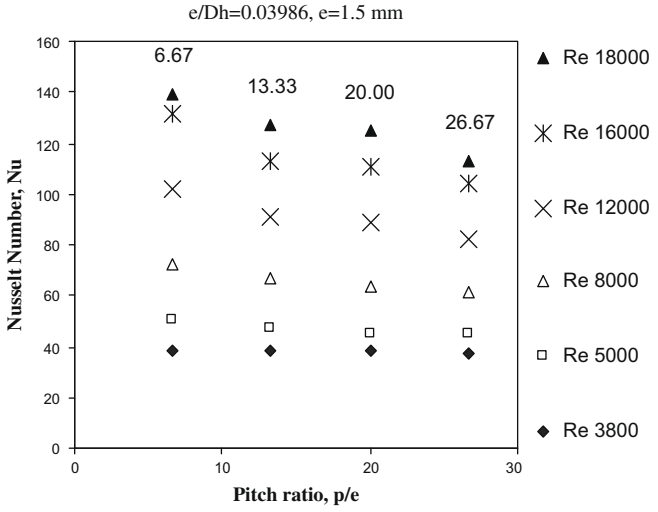

Fig. 12. Nusselt number as a function of roughness pitch for $e/D_h = 0.03986$.

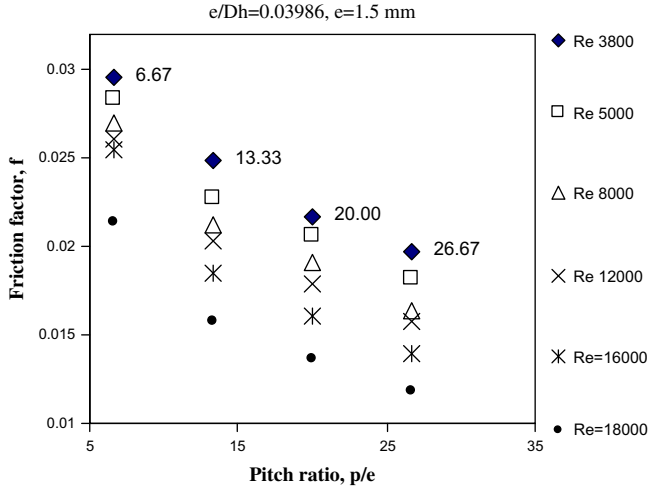

Fig. 13. Friction factor as a function of roughness pitch for $e/D_h = 0.03986$.

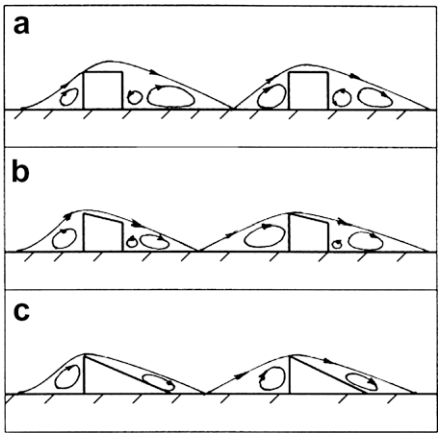

Fig. 14. Approximate model of flow pattern for (a) square, (b) chamfer rib and (c) wedge ribs geometry [11].

rib, intensity of eddies formation can be reduced as shown in Fig. 14 (c) i.e. with wedge shape ribs [11]. A thin inclined U-turbulator geometry with a passage underside as shown in Fig. 15, could definitely prevent totally the formation of eddies and also the redevelopment of two boundary layers at the reattachment point in between two adjacent ribs.

2. In case of ribs, shearing of boundary layer takes place only at its top-edge. The sharper the edge of ribs more will be the heat transfer rate and friction penalty too. Turbulator is having more number of sharp edges in order to shear more the viscous boundary layer. Two horizontal edges can form two free shear layers which either mix-up downstream with the accelerated flow (underway of turbulator) and create turbulences or form two reattachment points at the hot surface in order to enhance the heat transfer rate; that depends on the flow Reynolds number. Four side edges create a secondary flow may also interrupt the growth of the boundary layer which ultimately enhances the heat transfer coefficient.
3. As distance from the surface increases air velocity increases parabolically, it is expected that a somewhat higher velocity air flowing above the viscous sub-layer is obstructed and diverted towards the hot surface, to accelerate the stagnant air. This may be one of the reasons for maximum heat transfer enhancement at lower pitches.

However, this turbulator geometry is prepared not only to limit the pressure loss but also to increase the heat transfer coefficient by employing a gradual flow diversion technique in order to accelerate and shear the viscous flow. Height of the turbulator tip, $e = 1.5$ mm was limited by the friction penalty during experimentation. It was observed that the rate of increment of heat transfer is comparatively less than the rate of increment of friction factor for increasing turbulator tip heights as shown in the Table 3. The pitch-height ratio ($p/e = 6.67$) is limited by the size of the turbulator. It was also observed that the value of friction factor reduces with increasing values of roughness pitches attributed to less number of interruptions in the flow path.

The variation of Nusselt number and friction factor with relative roughness height is shown in Figs. 16 and 17. These figures show a continuous rise in the values of Nusselt number and friction factor with an increase in the turbulator tip height ratio, for the selected range of flow and roughness parameters. It can be seen that for a higher value of turbulator height ratio, the enhancement in heat transfer is higher at higher Reynolds num-

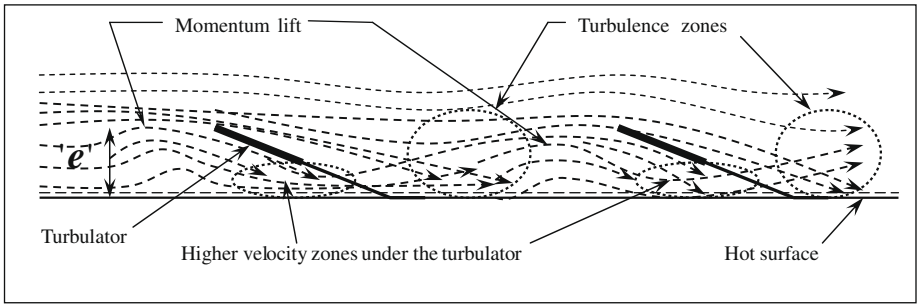

Fig. 15. Approximate anticipated flow pattern in case of present geometry.

Table 3
Enhancement ratio and friction factor ratio at turbulator pitches of 10, 20, 30 and 40 mm.

D_h = 37.63 mm				Enhancement ratio, Nu_r/Nu_s					
p	e	e/D_h	p/e	*Re* 3800	*Re* 5000	*Re* 8000	*Re* 12,000	*Re* 16,000	*Re* 18,000
10	0.7	0.0186012	14.285714	1.4225298	1.6700056	1.6537804	1.7682704	1.7503068	1.8049556
10	1	0.0265731	10	1.9731923	2.2771595	2.0788953	2.1865675	2.2552697	2.2608897
10	1.5	0.0398597	6.6666667	2.3882386	2.7855121	2.5544227	2.7535297	2.818676	2.8218623
20	0.7	0.0186012	28.571429	1.6969064	1.8460413	1.7321712	1.8094224	1.8471569	1.8884439
20	1	0.0265731	20	1.9575597	2.0502421	1.9395575	1.995058	2.0224	2.0920704
20	1.5	0.0398597	13.333333	2.3870445	2.598389	2.3396838	2.4472712	2.4373094	2.5694274
30	0.7	0.0186012	42.857143	1.5470445	1.8076395	1.7226641	1.9330189	1.9836496	2.0126685
30	1	0.0265731	30	1.8732348	2.1157561	1.9951917	2.2488374	2.087531	2.1706633
30	1.5	0.0398597	20	2.3696466	2.4861867	2.2145118	2.386476	2.3792941	2.5311984
40	0.7	0.0186012	57.142857	1.4172701	1.6667045	1.5940206	1.754251	1.6655059	1.7492121
40	1	0.0265731	40	1.8316952	2.0064252	1.8854987	2.0039412	1.9568677	1.9833522
40	1.5	0.0398597	26.666667	2.3342852	2.4962899	2.1574456	2.229007	2.2305882	2.2847465
				Friction factor ratio, f_r/f_s					
p	e	e/D_h	p/e	*Re* 3800	*Re* 5000	*Re* 8000	*Re* 12,000	*Re* 16,000	*Re* 18,000
10	0.7	0.0186012	14.285714	1.3333333	1.5	1.2727273	1.3809524	1.483871	1.4558824
10	1	0.0265731	10	1.7	2.2	1.9090909	2.1428571	2.3258065	2.3235294
10	1.5	0.0398597	6.6666667	2.5	3.125	2.7727273	3.1428571	3.7096774	3.7205882
20	0.7	0.0186012	28.571429	1.1666667	1.4	1.1818182	1.3095238	1.3870968	1.3529412
20	1	0.0265731	20	1.6	1.875	1.5545455	1.7142857	1.8064516	1.7970588
20	1.5	0.0398597	13.333333	2.1	2.5	2.1818182	2.452381	2.6806452	2.6470588
30	0.7	0.0186012	42.857143	1.1	1.35	1.1636364	1.247619	1.3225806	1.3235294
30	1	0.0265731	30	1.3666667	1.8	1.5363636	1.6666667	1.7677419	1.7647059
30	1.5	0.0398597	20	1.8333333	2.275	1.9545455	2.152381	2.3290323	2.2941176
40	0.7	0.0186012	57.142857	1.0666667	1.35	1.1363636	1.2	1.2612903	1.25
40	1	0.0265731	40	1.3333333	1.625	1.3636364	1.4761905	1.5645161	1.5294118
40	1.5	0.0398597	26.666667	1.6666667	2	1.6818182	1.9047619	2.0322581	1.9852941

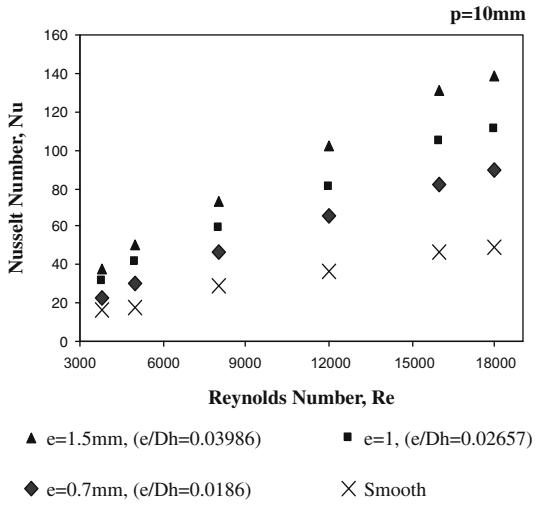

Fig. 16. Nusselt number as a function of Reynolds number at p = 10 mm.

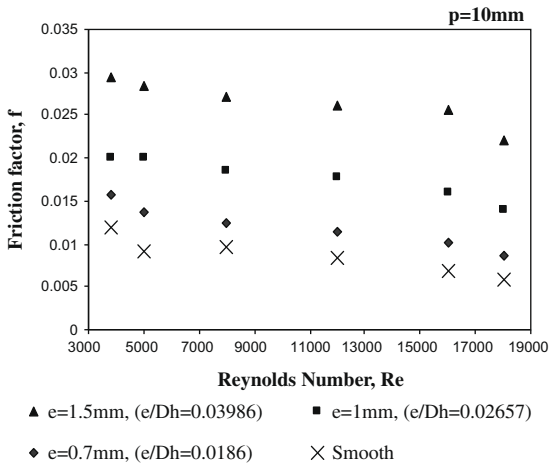

Fig. 17. Friction factor as function of reynolds number at p = 10 mm.

ber. Similar trend is observed in the literature. The maximum enhancement in Nusselt number and friction factor values compared to smooth duct are of the order of 2.82 and 3.72, respectively.

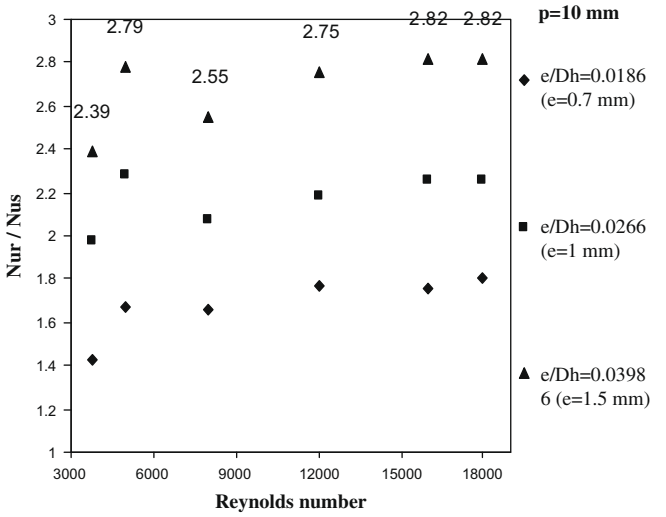

Fig. 18. Enhancement ratio as a function of Reynolds number for various roughness heights.

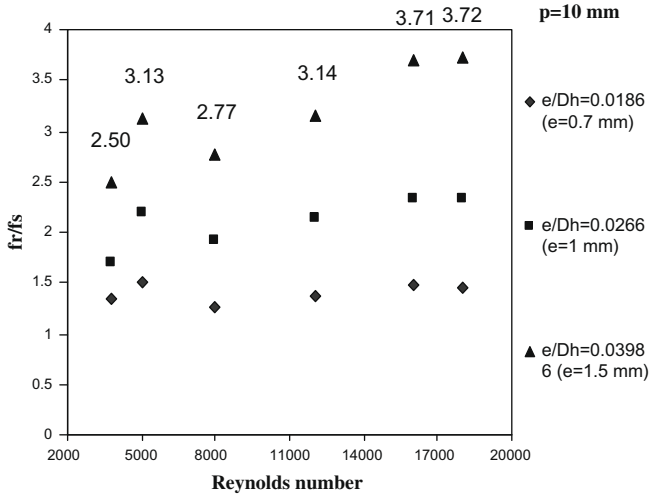

Fig. 19. Friction factor ratio as a function of '*Re*' for various roughness heights.

From the Figs. 18 and 19, it was seen that at a Reynolds number, $Re = 8000$, at which flow changes from transition to fully turbulent flow, a sudden drop in Nusselt number and friction factor takes place. Flow beyond this '*Re*' shows rise in the performance parameters. For roughened surface, at low Reynolds number ($Re = 3800$) and higher Reynolds number ($Re = 18{,}000$) heat transfer enhancement is 2.388 and 2.82 times smooth duct whereas friction penalty is 2.50 and 3.72, respectively.

4.2. Thermo-hydraulic performance and comparison with previous investigators

The performance curves have shown in Fig. 20. It was observed that, compared to smooth duct, the turbulators with $e = 1.5$ mm and $p = 10$ mm (i.e. $p/e = 6.67$) gave better thermo-hydraulic performance for the studied range of Reynolds number. The present geometry shows better thermo hydraulic performance in comparison to previous investigations using transverse and 60° inclined ribs, as seen from Fig. 21. For the above comparison, the approximate data of Fig. 21 is collected from page 3391, Fig. 12 of Abdul-Malik et al. [8] and page 493, Fig. 12 of Chandra et al. [20].

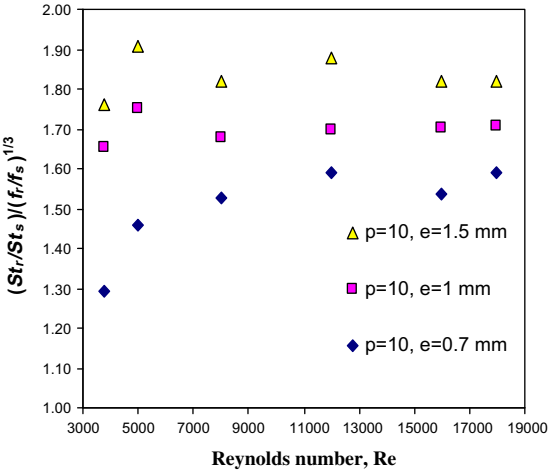

Fig. 20. Variation of performance parameter with *Re* for the specified roughness height ratio, 'e/D_h'.

Nusselt number and friction factor data of present work is compared with that of Bhagoria (page 358 of [11]) for the optimum transverse rib wedge angle, $\varphi = 10°$, and for the whole range of Reynolds number ($Re = 3212$–$17{,}594$) and also with Saini and Verma [18] using dimples as a roughness element; can be seen from Figs. 22 and 23. The flow direction in cases, present turbulator and wedge shaped ribs, was transverse (angle of attack of flow, $\alpha = 90°$). The data was compared for common roughness pitch-height ratio, $p/e = 10$. It was observed that the present geometry is superior to that of wedge ribs and of dimples, yielding better heat transfer enhancement at affordable friction penalty in the studied range of roughened flow and geometrical parameters. The comparison with other geometries available in the literature is also presented in Table 4.

4.3. Correlations for Nusselt number and friction factor

From Figs. 7–19 it can be concluded that the Nusselt number and friction factor are strong functions of geometric and operating parameters of roughened duct, namely the Reynolds number (Re), pitch to height ratio (p/e) and turbulator height ratio (e/D_h). The functional relationships for Nusselt number and friction factor can therefore be written as:

$$Nu_r = f(Re,\ p/e,\ e/D_h) \tag{9}$$

$$f_r = f(Re,\ p/e,\ e/D_h) \tag{10}$$

The data corresponding to all the 12 roughened plates totaling 72 data points were used for regression analysis. Fig. 24 shows the Nusselt number as a function of Reynolds number. A regression analysis to fit a straight line through these data points as:

$$Nu_r = A_o \times Re^{0.7054} \tag{11}$$

Since, the constant (A_o) will be a function of other parameters i.e. pitch-height ratio, (p/e). So, [$A_o = Nu_r/Re^{0.7054}$] is plotted in Fig. 25 as a function of pitch-height ratio and by regression analysis it was obtained as:

$$Nu_r/Re^{0.7054} = B_o \times (p/e)^{-0.1592} \tag{12}$$

Further, the constant (B_o) will be a function of roughness height ratio, (e/D_h) of turbulator.

So, the values of $Nu_r/(Re^{0.7054} \times (p/e)^{-0.1592})$ are plotted in Fig. 26 as a function of (e/D_h). It was obtained as, $Nu_r/[Re^{0.7054} \times (p/e)^{-0.1592}] = 0.5429 \times (e/D_h)^{0.3619}$.

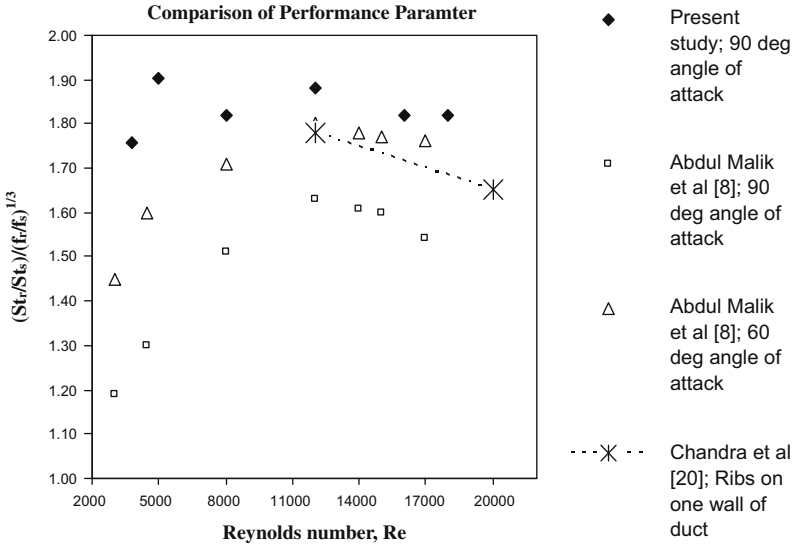

Fig. 21. Comparison of performance parameter, 'η' between present studies, Abdul et al. [8] and Chandra et al. [20].

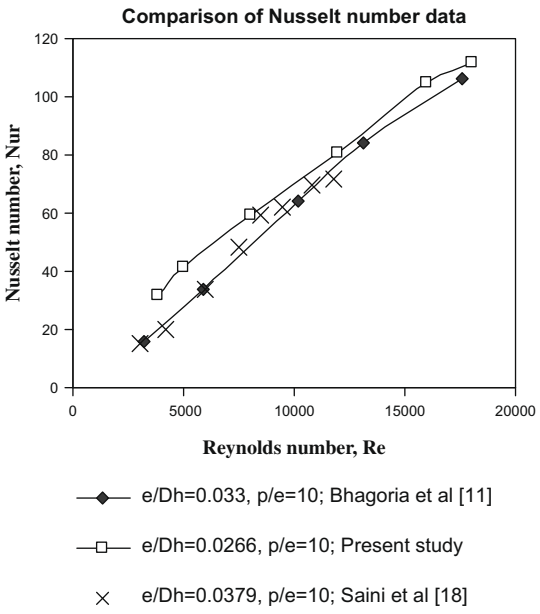

Fig. 22. Comparison of Nusselt number, 'Nu_r' amongst present studies, Bhagoria et al. [11] and Saini and Verma [18].

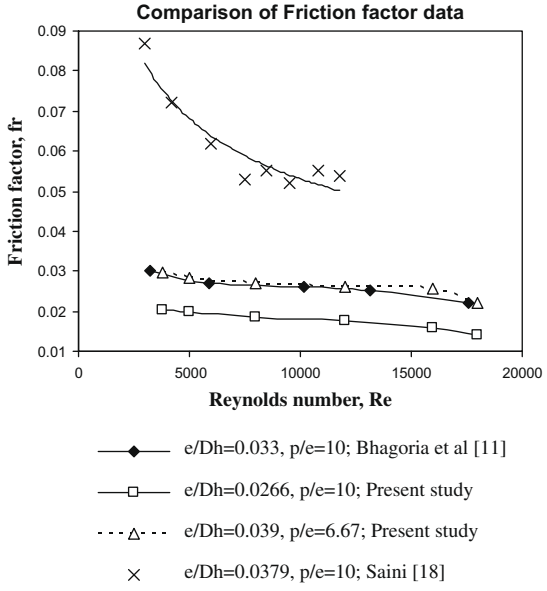

Fig. 23. Comparison of friction factor, 'f_r' amongst the present studies, Bhagoria et al. [11] and Saini and Verma [18].

The same correlation can be expressed as,

$$Nu_r = 0.5429 \times Re^{0.7054} \times (p/e)^{-0.1592} \times (e/D_h)^{0.3619} \quad (13)$$

Fig. 27 shows the plot of experimental values and the values predicted using Eq. (13). It can be seen that 91.67% of the data points (66 out of 72) lie within the deviation of ±25%. A similar procedure has been employed and a correlation for friction factor has been developed. Figs. 28–30 have been used to develop the following correlation:

$$f_r = 1.2134 \times Re^{-0.2076} \times (p/e)^{-0.4259} \times (e/D_h)^{0.3285} \quad (14)$$

Fig. 31 shows the plot of experimental values and the values predicted using Eq. (14) for friction factor. It can be seen that 91.67% of the data points (66 out of 72) for friction factor lie within the deviation of ±20%. Thus, the correlations developed are satisfactory for the prediction of the Nusselt number and friction factor of roughened duct with fairly good accuracy in the range of parameters investigated. It can be seen from Eqs. (13) and (14) the effect of Reynolds number on the Nusselt number and that of turbulator pitch on the friction factor of the turbulator roughened duct is much stronger as compared to that of other parameters. More number of turbulators causing shearing or breaking of viscous layer at more number of locations resulting increase in friction penalty. Hence, with present turbulator, roughness pitch has higher influence on friction factor in the roughened duct.

Another notable difference lies in the effect of turbulator tip height ratio; the influence being same in both, Nusselt number and friction factor. As the turbulator tip height increases, the tendency of higher velocity air to approach the surface increases that results better heat transfer enhancement and more obstruction in the turbulent core causes more friction factor.

Table 4
Comparison of performance parameter $(Nu_r/Nu_s)/(f_r/f_s)^{1/3}$ for various roughness geometries.

Sr. No.	References	Geometry	Parameters		Nu_r/Nu_s	f_r/f_s	$(Nu_r/Nu_s)/(f_r/f_s)^{1/3}$
1	Prasad and Saini [3]	Transverse wire	*Re*: 5000–50000 e/D_h: 0.02–0.033	*p*/*e* 10 *p*/*e* 15 *p*/*e* 20	2.38 2.14 2.01	2.38 2.14 2.92	**1.78** **1.66** **1.41**
2	Abdul et al. [8]	V-shaped wire Ribs 60° angle of Attack	*Re*: 2500–18000 e/D_h: 0.02–0.034 *p*/*e*: 10, α = 30–90°		2.3	2.83	**1.63**
3	Bhagoria et al.[11]	Transverse Wedge shape rib Roughness	*Re*: 3000–18000 e/D_h: 0.015– 0.033 *p*/*e*: 7.57–12.12 Φ: 8–15 deg		2.4	5.3	**1.38**
4	Jaurker et al. [12]	Rib-groove Roughness	*Re*: 3000–21000 e/D_h: 0.018–0.036 *p*/*e*: 4.5–10 g/p: 0.3–0.7		2.7	3.6	**1.76**
5	Saini and Saini [13]	Expanded wire Mesh	*Re*: 1900–13000 e/D_h: 0.012–0.039 L/e: 25–71.87 S/e: 15.62–46.87		4	5	**2.34**
6	Karmare and Tikekar [15]	Square grit ribs (Staggered) α = 60°	*Re*: 4000–17000 e/D_h: 0.035–0.044 *p*/*e*: 12.5–36 l/s: 1.72–1		2	3	**1.39**
7	**Present study**	Inverted	e/D_h: 0.018–0.039 *p*/*e*: 6.67–57.14, α = 90°				
		U-shaped Turbulator	At, *Re* = 18000 At, *Re* = 3800		2.82 2.388	3.72 2.50	**1.82** **1.76**

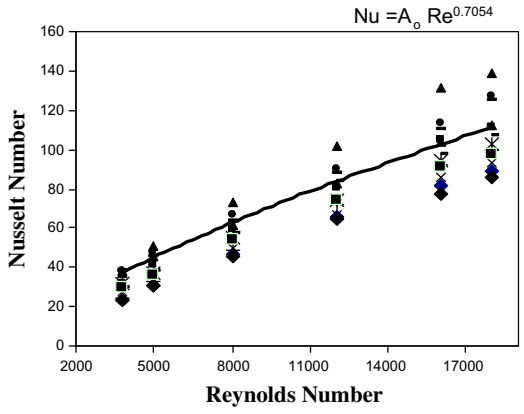

Fig. 24. Variation of '*Nu*' as a function of '*Re*'.

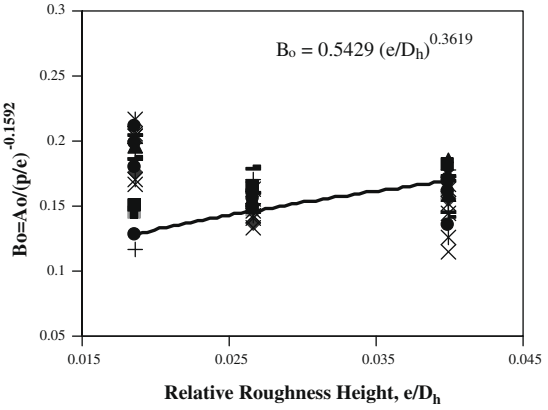

Fig. 26. Plot of $B_o = Nu_r/(Re^{0.7054} \times (p/e)^{-0.1592})$.

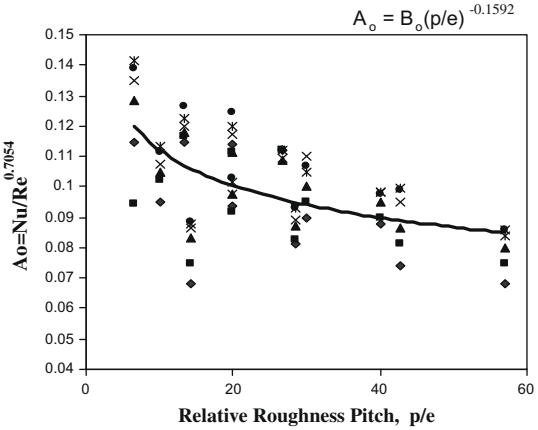

Fig. 25. Plot of $A_o = Nu_r/Re^{0.7054}$ vs. pitch ratio '*p*/*e*'.

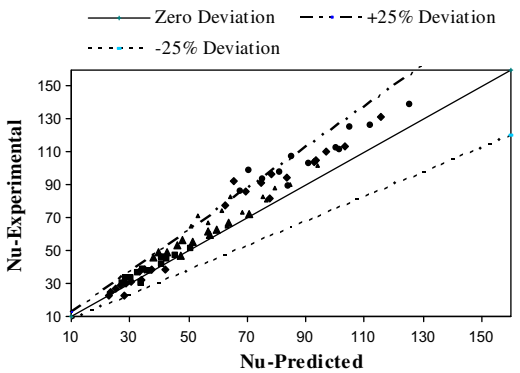

Fig. 27. Plot of '$Nu_{experimental}$' vs. '$Nu_{predicted}$'.

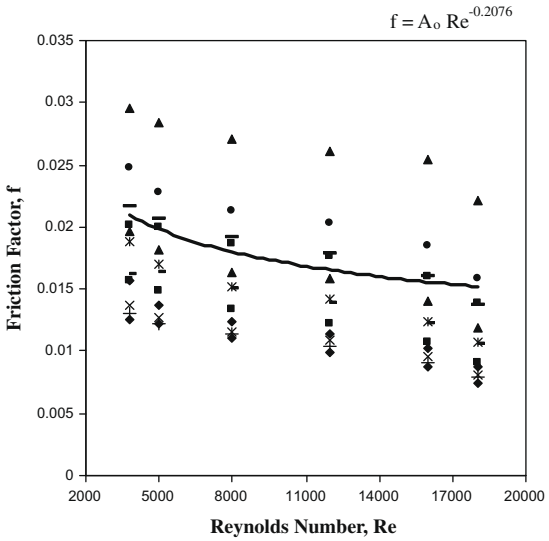

Fig. 28. Plot of friction factor vs. Reynolds number.

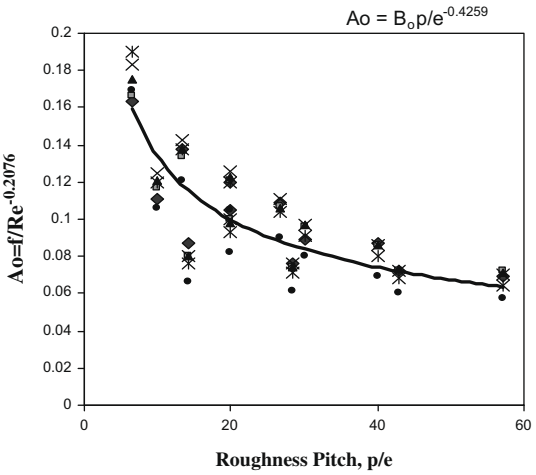

Fig. 29. Plot of '$f/Re^{-0.2076}$' vs. pitch ratio, 'p/e'.

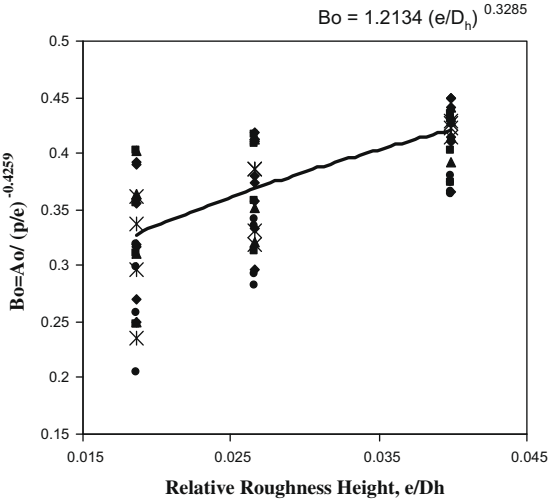

Fig. 30. Plot of '$f/[Re^{-0.2076} \times (p/e)^{-0.4259}]$' vs. pitch ratio, '$p/e$'.

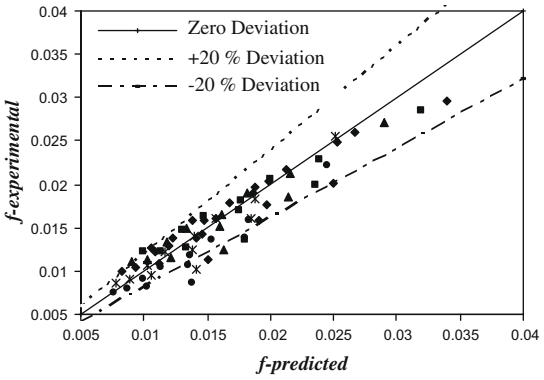

Fig. 31. Plot of '$f_{experimental}$' vs. '$f_{predicted}$'.

5. Conclusions

An experimental study of the flow of air in a rectangular duct with one roughened wall with 'inverted U-shaped turbulators', subjected to uniform heat flux boundary condition has been performed. The remaining three smooth walls were insulated. These conditions correspond to the flow in the solar air heater duct. The effect of Reynolds number, relative roughness pitch and relative roughness height on the heat transfer coefficient and friction factor has been studied. Results have been compared with those of a smooth duct under similar flow conditions to determine enhancement in heat transfer coefficient and friction factor. Investigations have been carried out in medium Reynolds number flow (Re = 3800–18,000). Following conclusions have been drawn:

(a) Roughness pitch strongly affects the flow pattern and hence the performance of the duct. The turbulator geometry shows appreciable heat transfer enhancement even at low Reynolds number too (Re < 5000) where ribs are inefficient. At Reynolds number, Re = 3800, the maximum enhancement in Nusselt number and friction factor are of the order of 2.388 and 2.50, respectively.
(b) The maximum enhancement in Nusselt number and friction factor values compared to smooth duct (in this medium 'Re' flow range of investigation at pitch of about 10 mm and turbulator tip height of 1.5 mm) are of the order of 2.82 and 3.72, respectively.
(c) The turbulences generated only in the viscous sub-layer region of boundary layer results in better thermo-hydraulic performance i.e. maximum heat transfer enhancement at affordable friction penalty.

Acknowledgement

This work has been carried out at the Mechanical Engineering Department, Dr. Babasaheb Ambedkar Technological University, Lonere 402103 (Raigad), Maharashtra, India. The authors acknowledge this university for providing financial assistance for this research.

References

[1] M.Y. Salam, Measurement of the viscous sublayer in near-separated flows, Applied Scientific Research 39 (1982) 337–347.
[2] J.C. Han, L.R. Glicksman, W.M. Rohsenow, An investigation of heat transfer and friction for rib roughened surfaces, International Journal of Heat and Mass Transfer 21 (1978) 1143–1156.

[3] B.N. Prasad, J.S. Saini, Effect of artificial roughness on heat transfer and friction factor in a solar air heater, Solar Energy 41 (6) (1988) 555–560.
[4] Dhananjay Gupta, S.C. Solanki, J.S. Saini, Heat and fluid flow in rectangular solar air ducts having transverse rib roughness on absorber plates, Solar Energy 51 (1) (1993) 31–37.
[5] S.K. Verma, B.N. Prasad, Investigation for the optimal thermo hydraulic performance of artificially roughened solar air heaters, Renewable Energy (20) (2000) 19–36.
[6] D. Gupta, S.C. Solanki, J.S. Saini, Thermo hydraulic performance of solar air heaters with roughened absorber plates, Solar Energy 61 (1) (1997) 33–42.
[7] M.M. Sahu, J.L. Bhagoria, Augmentation of heat transfer coefficient by using 90° broken transverse ribs on absorber plate of solar air heater, Renewable Energy (30) (2005) 2057–2073.
[8] Abdul-Malik Ebrahim Momin, J.S. Saini, S.C. Solanki, Heat transfer and friction in solar air heater duct with V-shaped rib roughness on absorber plate, International Journal of Heat and Mass Transfer (45) (2002) 3383–3396.
[9] Alok Chaube, P.K. Sahoo, S.C. Solanki, Analysis of heat transfer augmentation and flow characteristics due to rib roughness over absorber plate of a solar air heater, Renewable Energy (31) (2006) 317–331.
[10] A. Layek, J.S. Saini, S.C. Solanki, Heat transfer and friction characteristics of solar air heater having compound turbulator on absorber plate, National conference on Advances in Energy Research, (4th–5th Dec. 2006), IIT-Bombay, India.
[11] J.L. Bhagoria, J.S. Saini, S.C. Solanki, Heat transfer coefficient and friction factor correlations for rectangular solar air heater duct having transverse wedge shaped rib roughness on the absorber plate, Renewable Energy (25) (2002) 341–369.
[12] A.R. Jaurker, J.S. Saini, B.K. Gandhi, Heat transfer and friction characteristics of rectangular solar air heater duct using rib-grooved artificial roughness, Solar Energy (80) (2006) 895–907.
[13] R.P. Saini, J.S. Saini, Heat transfer and friction factor correlations for artificially roughened ducts with expanded metal mesh as roughness element, International Journal of Heat and Mass Transfer 40 (4) (1997) 973–986.
[14] R. Karwa, S.C. Solanki, J.S. Saini, Heat transfer coefficient and friction factor correlations for the transitional flow regime in rib-roughened rectangular ducts, International Journal of Heat and Mass Transfer (42) (1999) 1597–1615.
[15] S.V. Karmare, A.N. Tikekar, Heat transfer and friction factor correlation for artificially roughened duct with metal grit ribs, International Journal of Heat and Mass Transfer (50) (2007) 4342–4351.
[16] K.R. Aharwal, B.K. Gandhi, J.S. Saini, Experimental investigation on heat transfer enhancement due to gap in an inclined continuous rib arrangement in a rectangular duct of solar air heater, Renewable Energy (33) (2008) 585–596.
[17] A.C. Pfahnl, J.H. Lienhard, A.H. Stocum, Heat Transfer enhancing features for handler tray device carriers, IEEE Transactions of Components Packaging and Manufacturing Technology (21) (1998) 302–310.
[18] R.P. Saini, J. Verma, Heat transfer and friction factor correlations for a duct having dimple-shape artificial roughness for solar air heaters, Energy (33) (2008) 1277–1287.
[19] B.N. Prasad, J.S. Saini, Optimal thermo hydraulic performance of artificially roughened solar air heaters, Solar Energy 47 (2) (1991) 91–96.
[20] P.R. Chandra, C.R. Alexander, J.C. Han, Heat transfer and friction factor behaviors in rectangular channels with varying number of ribbed walls, International Journal of Heat and Mass Transfer (46) (2003) 481–495.
[21] J.C. Han, J.S. Park, Developing heat transfer in rectangular channels with rib turbulators, International Journal of Heat and Mass Transfer 31 (1) (1988) 183–195.
[22] J.C. Han, Heat transfer and frictional characteristics in rectangular channels with rib turbulators, ASME Journal of Heat Transfer 110 (1988) 321–328.
[23] J.C. Han, S. OU, J.S. Park, C.K. Lei, Augmented heat transfer in rectangular channels of narrow aspect ratios with rib turbulators, International Journal of Heat and Mass Transfer 32 (9) (1989) 1619–1630.
[24] J.S. Park, J.C. Han, Y. Huang, S. Ou, Heat Transfer performance comparisons of five different rectangular channels with parallel angled ribs, International Journal of Heat and Mass Transfer 35 (11) (1992) 2891–2903.
[25] Y.M. Zhang, W.Z. Gu, J.C. Han, Heat transfer and friction in rectangular channels with ribbed or ribbed-grooved walls, ASME Journal of Heat Transfer (116) (1994) 58–65.
[26] T.M. Liou, J.J. Hwang, Effect of ridge shapes on turbulent heat transfer and friction in a rectangular channel, International Journal of Heat and Mass Transfer 36 (4) (1993) 931–940.
[27] R. Kiml, S. Mochizuki, A. Murata, Effects of rib arrangements on heat transfer and flow behavior in a rectangular rib-roughened passage: application to cooling of gas turbine blade trailing edge, ASME Journal of Heat Transfer (123) (2001) 675–681.
[28] S.C. Lau, R.D. McMillin, J.C. Han, Turbulent heat transfer and friction in a square channel with discrete rib turbulators, ASME Journal of Heat Transfer (113) (1991) 360–366.
[29] T.M. Liou, J.J. Hwang, Turbulent heat transfer augmentation and friction in periodic fully developed channel flows, ASME Journal of Heat Transfer (114) (1992) 56–63.
[30] M.E. Taslim, L.A. Bondi, D.M. Kercher, An experimental investigation of heat transfer in an orthogonally rotating channel roughened with 45° criss–cross ribs on two opposite walls, ASME Journal of Heat Transfer (113) (1991) 346–353.
[31] J.C. Han, Y.M. Zhang, High performance heat transfer ducts with parallel broken and V-shaped broken ribs, International Journal of Heat and Mass Transfer 35 (2) (1992) 513–523.
[32] S.C. Lau, R.D. McMillin, J.C. Han, Heat transfer characteristics of turbulent flow in a square channel with angled discrete ribs, Journal of Turbomachinery (113) (1991) 367–374.
[33] M.E. Taslim, T. Li, D.M. Kercher, Experimental heat transfer and friction in channels roughened with angled, V-shaped and discrete ribs on two opposite walls, ASME Journal of Heat Transfer (118) (1996) 20–28.
[34] G. Tanda, Heat transfer in rectangular channels with transverse and V-shaped broken ribs, International Journal of Heat and Mass Transfer (47) (2004) 229–243.
[35] P.M. Ligrani, G.I. Mahmood, J.L. Harrison, C.M. Clayton, D.L. Nelson, Flow structure and local Nusselt number variations in a channel with dimples and protrusions on opposite walls, International Journal of Heat and Mass Transfer (44) (2001) 4413–4425.
[36] N.K. Burgess, M.M. Oliveira, P.M. Ligrani, Nusselt number behavior on deep dimpled surfaces within a channel, ASME Journal of Heat Transfer (125) (2003) 11–18.
[37] S.W. Chang, T.M. Liou, M.H. Lu, Heat transfer of rectangular narrow channel with two opposite scale roughened walls, International Journal of Heat and Mass Transfer (48) (2005) 3921–3931.
[38] K. Katoh, K. Choi, T. Azuma, Heat transfer enhancement and pressure loss by surface roughness in turbulent channel flows, International Journal of Heat and Mass Transfer (43) (2000) 4009–4017.
[39] E.H. Ridouane, A. Campo, Heat transfer enhancement of air flowing across grooved channels: joint effects of channel height and groove depth, ASME Journal of Heat Transfer (130) (2008). 02901-1-7.
[40] H. Kim, K. Kim, Design optimization of rib-roughened channel to enhance turbulent heat transfer, International Journal of Heat and Mass Transfer (47) (2004) 5159–5168.
[41] S.B. Bopche, M.S. Tandale, International Conference on Advances in Energy Research (Dec. 12–14), IIT-Bombay, India, 2007.
[42] J.A. Duffie, W.A. Beckman, Solar Engineering of Thermal Processes, Wiley, New York, 1980.